arXiv:1612.08798v1 [cond-mat.quant-gas] 28 Dec 2016

# Bifurcations, stability, and mode evolution in segregated condensate mixtures

Sukla Pal, Arko Roy, and D. Angom
*Physical Research Laboratory, Ahmedabad-380009, Gujarat, India*

We present new features of low energy Bogoliubov quasiparticle excitations of a two component Bose-Einstein condensate (TBEC) in quasi-2D geometry at zero temperature using Hartree-Fock-Bogoliubov (HFB). We, in particular, consider the TBECs of $^{133}$Cs -$^{87}$Rb and $^{85}$Rb -$^{87}$Rb, and show specific features in the low energy excitation spectrum as a function of the interaction strength. For $^{85}$Rb -$^{87}$Rb TBEC, the appearance of a new zero energy mode is observed. Whereas for $^{133}$Cs -$^{87}$Rb TBEC we report a bifurcation of the softened Kohn mode at the point of transition from miscible to immiscible domain. The lower energy mode, after the bifurcation, goes soft and becomes a new Goldstone mode of the system.

PACS numbers: 03.75.Mn,03.75.Hh,67.60.Bc,67.85.Bc

## I. INTRODUCTION

The study of quasi-low-dimensional systems is the key to understand intriguing aspects in the physics of ultracold atoms. It is often observed that the dynamics and the characteristic properties of the excitations change significantly with dimension. In this regard, the trapped two-component Bose-Einstein condensates (TBECs) are interesting systems to explore. By choosing trapping parameters properly, the system can be made quasi-low-dimensional and manipulate the atomic interactions as well. Apart from these, the possibility of transition from miscible to immiscible phase makes the TBECs even more fascinating. At zero temperature, under Thomas-Fermi (TF) approximation the condition of phase separation in TBEC is given by the inequality $U_{12}^2 > U_{11}U_{22}$ [1, 2]; where $U_{11}$ and $U_{22}$ are the intraspecies and $U_{12}$ is the interspecies interaction strength. With immense experimental achievements, the realization of TBEC has been possible for several BEC mixtures of which $^{85}$Rb -$^{87}$Rb [3] and $^{133}$Cs -$^{87}$Rb [4] TBEC are considered as representative examples in this present work, and examined in detail. In particular, the observation of phase separation in $^{85}$Rb -$^{87}$Rb [5, 6] and $^{87}$Rb -$^{133}$Cs [7] TBEC has opened new directions for various theoretical investigations in mixed systems. Among various theoretical formalisms, Hartree-Fock-Bogoliubov theory with Popov approximation (HFB-Popov) [8–10] has been used satisfactorily in case of single-species BEC to account for the finite temperature effects in mode energies [9, 11] of collective excitations. Besides these, it also possible to study the dynamical instabilities [12, 13] in $^{85}$Rb -$^{87}$Rb TBEC at zero temperature. Being a gapless theory, HFB-Popov is of special interest in studying excitation spectrum and till now has gained much attention in illustrating the physics of collective excitations. Recently, the study has been extended for cigar-shaped TBEC in miscible [14] and in phase-separated domain [15–17]. Also, in quasi-2D condensate of $^{23}$Na, this theory has been successfully applied [18] to show the modification in the excitation spectrum due to transformation of trapping geometry at zero temperature. Therefore, at this point it is natural to explore the new features associated with the mode evolution spectrum in quasi-2D TBEC. Keeping this aim in mind, in this article, we apply HFB-Popov approximation and study systematically the evolution of low energy eigenmodes of Bogoliubov-de-Gennes (BdG) equations [19, 20] in $^{85}$Rb -$^{87}$Rb and $^{133}$Cs -$^{87}$Rb TBEC to obtain the change in quasiparticle excitation energy of the pancake-shaped condensate at zero temperature. The BdG equations have already been used extensively in characterizing the excitations of TBEC across miscible to immiscible phase transition [21], and in finite temperature analysis of quasi-2D single component dipolar gas [22].

We have, in particular, chosen $^{85}$Rb -$^{87}$Rb TBEC to show the special features in excitation spectrum when two species in the TBEC have small mass difference. The fact that the background scattering length of $^{85}$Rb is negative, the BECs of $^{85}$Rb is achievable only after tuning the scattering length to positive values through Feshbach resonance [23, 24]. So, in this case, the TBEC is driven through the miscible-immiscible transition or vice-versa by tuning the intraspecies interaction of $^{85}$Rb. Most importantly, as it is the species with the lighter mass, it also leads to the observation of Rayleigh-Taylor instability (RTI) as the scattering length of $^{85}$Rb approaches and crosses the scattering length of $^{87}$Rb. The ground state of this TBEC in the immiscible domain shows shell structured density profile, and hence reflects the symmetry of the trapping potential. In contrast, $^{133}$Cs -$^{87}$Rb TBEC is made up of two alkali atoms with significant mass difference, and one has the scope to navigate the miscible-immiscible transition by changing either the intraspecies or interspecies interactions. In the present work we vary the interspecies interaction. As the interaction is increased, the TBEC undergoes the miscible-immiscible transition with the side-by-side density profiles as the preferred geometry. In both the TBECs there are softening of modes associated with the emergence of RTI and miscible-immiscible transition. However, the trends associated with the two phenomena are quite different. In the former case, the modes which go soft become zero energy modes, but in the latter, the soft modes leads to new Goldstone modes in the system.

The paper is organized as follows: In Sec. II we provide a brief description of the HFB-Popov formalism implemented for interacting quasi-2D TBEC. We then outline the numerical procedure employed to solve the Bogoliubov-de-Gennes equations in. The results and discussions pertaining to $^{85}$Rb-$^{87}$Rb and $^{133}$Cs -$^{87}$Rb condensate mixtures are given in Sec. III. The evolution of the quasiparticle excitation energies and amplitudes with variation in intraspecies scattering

length of $^{85}$Rb are presented in Sec. III A. Next, we discuss the variation in condensate density distribution and nature of mode evolution in $^{133}$Cs -$^{87}$Rb condensate mixture given in Sec. III B. We, then, end with conclusions highlighting the key findings of the present work in Sec. IV.

## II. THEORY

We consider a TBEC in an anisotropic trap with strong axial binding such that the frequencies of the harmonic trapping potential satisfy the condition $\omega_\perp \ll \omega_z$ with $\omega_x = \omega_y \equiv \omega_\perp$, a configuration which is also referred as pancake (disk) shaped. With this choice, the TBEC remains in the ground state along the axial direction, and degrees of freedom are frozen. The system is thus effectively in the quasi-two-dimensional regime where the excitations are only along the radial direction. Under the mean field approximation, to incorporate the effects of quantum fluctuations around the ground state at zero temperature, we resort to the second-quantized form of the grand-canonical Hamiltonian given by

$$\hat{H} = \sum_{k=1,2} \iint dxdy \hat{\Psi}_k^\dagger(x,y,t) \Bigg[ -\frac{\hbar^2}{2m_k}\nabla_\perp^2 + V_k(x,y) - \mu_k + \frac{U_{kk}}{2}\hat{\Psi}_k^\dagger(x,y,t)\hat{\Psi}_k(x,y,t)\Bigg]\hat{\Psi}(x,y,t) + \; U_{12}\iint dxdy \times \hat{\Psi}_1^\dagger(x,y,t)\hat{\Psi}_2^\dagger(x,y,t)\hat{\Psi}_1(x,y,t)\hat{\Psi}_2(x,y,t), \tag{1}$$

with $k = 1, 2$ as the species label, $\hat{\Psi}_k$ ($\hat{\Psi}_k^\dagger$) are the Bose field annihilation (creation) operators of the two species, and $\mu_k$s are the chemical potentials. The strength of the coupling constants are given by $U_{kk} = 2a_{kk}\sqrt{2\pi\lambda}$ and $U_{12} = 2a_{12}\sqrt{2\pi\lambda}(1 + m_1/m_2$. It is to be noted that for pancake shaped traps the anisotropy parameter, as mentioned earlier, $\lambda = \omega_z/\omega_\perp \gg 1$, and the form of the confining potential is $V(x,y,z) = (1/2)m\omega_\perp^2(x^2 + y^2 + \lambda^2 z^2)$. In the present work we consider $a_{kk}$ and $a_{12}$, the intraspecies and interspecies scattering lengths, respectively, to be positive (repulsive). In TBECs, an important phenomenon is the transition from miscible to immiscible phases or vice-versa. The miscible-immiscible transition is governed by the strength of the inter- and intraspecies interaction. Under the Thomas-Fermi approximation, the immiscible phase is characterized by the condition $U_{12}^2 > U_{11}U_{22}$ [1, 2, 25]. This inequality holds true when all the interactions in the TBEC are repulsive.

As the ground state is macroscopically occupied for the temperature regime pertinent to the experiments, the condensate part can be separated out from the Bose field operator through the Bogoliubov decomposition $\hat{\Psi}_k = \phi_k + \tilde{\psi}_k$, where $\phi_k = \langle\hat{\Psi}_k\rangle$s are the $c$-fields representing each of the condensate species, and $\tilde{\psi}_k$s are the corresponding non-condensate densities or fluctuations. These fluctuations may be either be quantum or thermal. Furthermore, using HFB-Popov approximation [8], $\phi_k$s are obtained as the stationary solutions of the coupled generalized Gross-Pitaevskii equations

$$\hat{h}_k\phi_k + U_{kk}\left[n_{ck} + 2\tilde{n}_k\right]\phi_k + U_{12}n_{3-k}\phi_k = 0, \tag{2}$$

where, $n_{ck}(x,y) \equiv |\phi_k(x,y)|^2$, $\tilde{n}_k(x,y) \equiv \langle\tilde{\psi}^\dagger(x,y,t)\tilde{\psi}(x,y,t)\rangle$ and $n_k(x,y) = n_{ck}(x,y) + \tilde{n}_k(x,y)$ represent the density of local condensate, non-condensate and total condensate respectively; $\hat{h}_k = (-\hbar^2/2m_k)\nabla_\perp^2 + V_k(x,y) - \mu_k$ is the one-body part of the grand canonical Hamiltonian presented in Eq. (1). In terms of quasiparticle modes the fluctuations represented by $\tilde{\psi}(x,y,t)$ are of the form

$$\tilde{\psi}_k = \sum_j \left[u_{kj}(x,y)\hat{\alpha}_j(x,y)e^{-iE_jt/\hbar} - v_{kj}^*(x,y)\hat{\alpha}_j^\dagger(x,y)e^{iE_jt/\hbar}\right] \tag{3}$$

where, $\hat{\alpha}_j$ ($\hat{\alpha}_j^\dagger$) are the quasiparticle annihilation (creation) operator satisfying Bose commutation relations, and is considered common to both the species. The subscript $j$ represents the energy eigenvalue index, and the functions $u_{jk}$ and $v_{jk}$ are the Bogoliubov quasiparticle amplitudes corresponding to $j$th energy eigen-state. The quasiparticle amplitudes are normalized as

$$\iint dxdy \sum_k \left(|u_k(x,y)|^2 - |v_k(x,y)|^2\right) = 1. \tag{4}$$

Using the above definitions and considerations, the Bogoliubov-de-Gennes equations for a TBEC system are [15, 21]

$$\hat{\mathcal{L}}_1 u_{1j} - U_{11}\phi_1^2 v_{1j} + U_{12}\phi_1\left(\phi_2^* u_{2j} - \phi_2 v_{2j}\right) = E_j u_{1j}, \tag{5a}$$
$$\underline{\hat{\mathcal{L}}}_1 v_{1j} + U_{11}\phi_1^{*2} u_{1j} - U_{12}\phi_1^*\left(\phi_2 v_{2j} - \phi_2^* u_{2j}\right) = E_j v_{1j}, \tag{5b}$$
$$\hat{\mathcal{L}}_2 u_{2j} - U_{22}\phi_2^2 v_{2j} + U_{12}\phi_2\left(\phi_1^* u_{1j} - \phi_1 v_{1j}\right) = E_j u_{2j}, \tag{5c}$$
$$\underline{\hat{\mathcal{L}}}_2 v_{2j} + U_{22}\phi_2^{*2} u_{2j} - U_{12}\phi_2^*\left(\phi_1 v_{1j} - \phi_1^* u_{1j}\right) = E_j v_{2j}, \tag{5d}$$

where $\hat{\mathcal{L}}_1 = \left(\hat{h}_1 + 2U_{11}n_1 + U_{12}n_2\right)$, $\hat{\mathcal{L}}_2 = \left(\hat{h}_2 + 2U_{22}n_2 + U_{12}n_1\right)$ and $\underline{\hat{\mathcal{L}}}_k = -\hat{\mathcal{L}}_k$. To solve the above eigenvalue equations, $u_{kj}$s and $v_{kj}$s are decomposed into a linear combination of harmonic oscillator eigenstates followed by the diagonalisation of the Bogoliubov-de-Gennes matrix (BdGM) constructed from Eq. 5. The order parameters $\phi_k$s and the non-condensate densities $\tilde{n}_k$s are then the self-consistent solutions of the coupled Eqns. (2) and (5). The thermal components, in terms of the quasiparticle amplitudes, are defined to be

$$\tilde{n}_k = \sum_j \left[(|u_{kj}|^2 + |v_{kj}|^2)N_0(E_j) + |v_{kj}|^2\right], \tag{6}$$

where, $N_0(E_j) = (e^{\beta E_j} - 1)^{-1}$ with $\beta = 1/(k_B T)$ is the Bose factor of the $j$th quasiparticle mode at temperature $T$. In the above expression the term $|v_{kj}|^2$, independent of $N_0(E_j)$ and hence, the temperature, represents the quantum fluctuations. As $T$ approaches zero, the role of thermal fluctuations diminishes, and at $T = 0$ the contribution from thermal fluctuations ceases completely since $N_0(E_j)$ in Eq.(6) vanishes. The non-condensate density is then governed by quantum fluctuations only as Eq. (6) reduces to $\tilde{n}_k = \sum_j |v_{kj}|^2$. Thus at finite temperatures the non-condensate density has dominant contribution from thermal fluctuations as well as quantum fluctuations.

To obtain the Bogoliubov quasiparticle amplitudes, we adopt following numerical scheme. At first, we numerically solve the pair of coupled GP Eqns. (2) using the split step Crank-Nicholson (CN) method. Using these solutions, the BdG Eqns. (5) are then cast as a matrix eigenvalue equation in the basis of the harmonic oscillator potential eigenstates. Then we write $u_k$ and $v_k$'s as linear combination of the harmonic oscillator direct product states $\varphi(x)\otimes\varphi(y)$, where $\varphi(x)$ and $\varphi(y)$ are the harmonic oscillator eigenstates in $x$ and $y$ direction, respectively. With this definition,

$$u_{1j}(x,y) = \sum_{k,l=0}^{N_b} p_{jkl}\varphi_{kj}(x)\varphi_{lj}(y) \tag{7}$$

where, $p_{jkl}$ is the coefficients of linear combination. Similarly, we can define $u_{2j}$, $v_{1j}$, and $v_{2j}$ as linear combinations of the direct product states. Using the above definition, for equal number of basis functions $N_b$ along the $x$ and $y$ axis, the BdG matrix is of dimension $4(N_b+1)(N_b+1)\times 4(N_b+1)(N_b+1)$. Considering the orthogonality of harmonic oscillator basis, the resulting BdG matrix is a sparse matrix. Due to the $N_b^2$ scaling of the BdG matrix, the matrix size rapidly increases with the basis size, and it is essential to use algorithms capable of large matrix diagonalization. For this reason we use ARPACK [26] routines to diagonalises the BdG matrix, and consequently, we consider a selected set of the quasiparticle amplitudes in the computation of fluctuations or non-condensate density. This is done such that, only the very high energy modes and hence, negligible Bose factor, quasiparticle amplitudes are excluded from the computation of non-condensate density. The non-condensate density is computed using the Eq. (6), and we iterate the solutions until the condensate, and non-condensate densities converge to the predefined accuracies. To accelerate the convergence we use the method of successive under-relaxation, and choose the under-relaxation parameter $S = 0.1$ [27]. The new solution at the $i$th iteration is then

$$\phi_i^{new}(x,y) = S\phi_i(x,y) + (1-S)\phi_{i-1}(x,y) \tag{8}$$

where $i$ is the iteration index. Since we focus on zero temperature excitations, the low energy eigenmodes will be sufficient to take care of the quasiparticle amplitudes.

## III. RESULTS AND DISCUSSIONS

The low-lying quasiparticle spectrum of a trapped quasi-2D TBEC is characterized by the presence of two Goldstone modes which appear due to breaking of $U(1)$ global gauge symmetry for each of the condensate species, and the Kohn modes [28–31]. The Kohn or dipole modes, among the low-lying energy eigenmodes have maximum $N_0$, and have the dominant contributions to the quantum fluctuations and thermal densities. For this reason, we investigate and examine the evolution of these modes, and in particular, study the topological deformation of the quasiparticle amplitude corresponding to the Kohn mode for various phases of the TBEC.

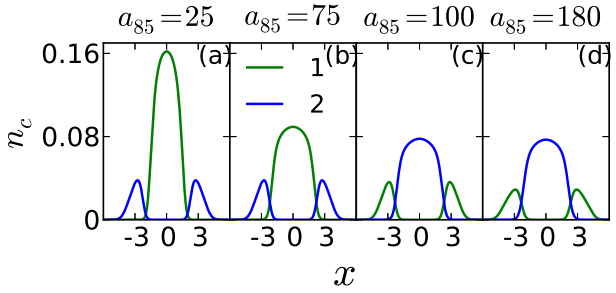


FIG. 1. (Color online)Equilibrium density profile of $^{85}$Rb-$^{87}$Rb along $x$-axis with $y = 0$ for $a_{^{85}\mathrm{Rb}}$ = 25, 75, 100, 180 $a_0$ at zero temperature. The density is measured in units of $a_{\mathrm{osc}}^{-2}$. (a)-(b) $^{85}$Rb condensate occupies the central region of the trap, and $^{87}$Rb condensate is at the edges. (c)-(d) As $a_{85}$ is increased when $a_{^{85}\mathrm{Rb}} > a_{^{87}\mathrm{Rb}}$, the density profiles switch their positions. The $x$ and $y$ are measured in units of $a_{\mathrm{osc}}$.

In the present study, we examine the evolution of the quasiparticle modes in TBEC systems with the variation in interaction strengths which drives the system from miscible to immiscible regime or vice-versa. The variation can either be the intra or the interspecies scattering length of the atoms constituting the TBEC. An representative example of the first possibility, tuning intraspecies interaction, is the TBEC of $^{85}$Rb - $^{87}$Rb, where the intraspecies scattering length of $^{85}$Rb can be tuned experimentally via a magnetic Feshbach resonance [5]. It must be mentioned here that, it is essential to tune the intraspecies scattering length of $^{85}$Rb as it has negative background scattering length. In this mixture, as the atomic masses are nearly same, the energetically favorable ground state configuration is the species with the lower repulsive interaction strength being surrounded by the species with higher repulsive interaction strength. The representative example of the other case, tuning the interspecies scattering length, is the TBEC of $^{133}$Cs -$^{87}$Rb, where the interspecies scattering length can be tuned through magnetic Feshbach resonance [4, 7]. In this case the stable ground state configuration is Cs atoms being surrounded by Rb atoms. We choose these representative systems and theoretically investigate the nature of excitation spectra in the miscible and immiscible phases of these systems at $T = 0$. Based on our previous works, the qualitative features of the results from these two examples are applicable to the TBECs of other possible atomic species.

### A. Mode evolution of $^{85}$Rb -$^{87}$Rb BEC mixture

To examine the quasiparticle excitation spectrum of $^{85}$Rb - $^{87}$Rb TBEC with our theoretical scheme, we consider $^{85}$Rb and $^{87}$Rb as species 1 and 2, respectively. The interspecies scattering length is $a_{12} = a_{^{85}\mathrm{Rb}-^{87}\mathrm{Rb}} = 214a_0$, where $a_0$ is the Bohr radius. Similarly, the intraspecies scattering lengths are denoted by $a_{22} = a_{^{87}\mathrm{Rb}}$, and $a_{11} = a_{85}$. In the present study, as mentioned earlier, we change $a_{11}$ while keeping $a_{22}$ fixed at $99a_0$. We consider equal number of particles for both the species $N_{^{85}\mathrm{Rb}} = N_{^{87}\mathrm{Rb}} = 5\times 10^3$, which maybe lower

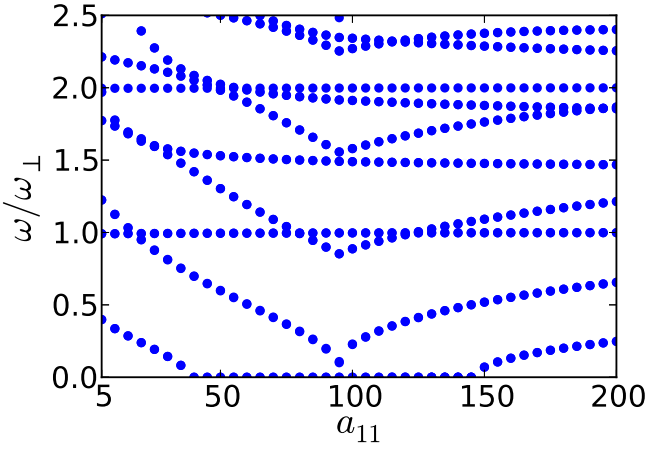


FIG. 2. (Color online) The evolution of low-lying mode energies as a function of $a_{11}$ in the domain $5a_0 \leqslant a_{11} \leqslant 200a_0$ at zero temperature for $N_1 = N_2 = 5000$. Here $a_{11}$ is in units of $a_0$.

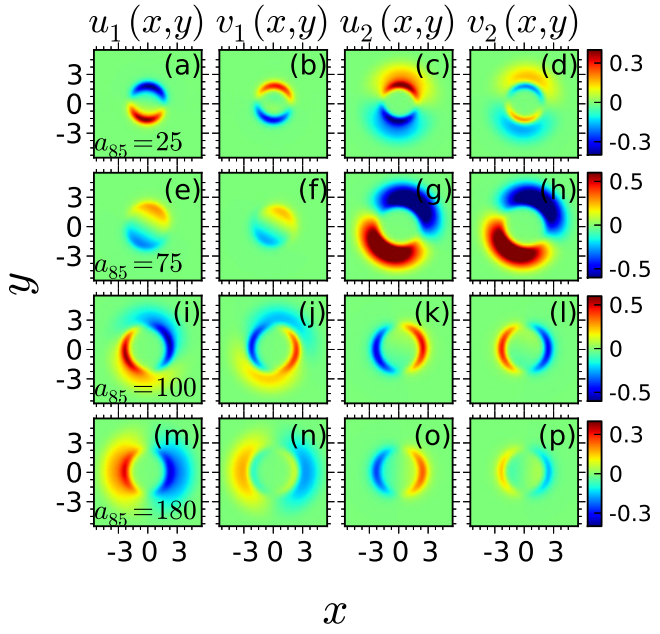


FIG. 3. (Color online) The Kohn mode amplitude at selected values of $a_{^{85}\mathrm{Rb}}$, and the other scattering lengths are kept fixed. The chosen values of $a_{^{85}\mathrm{Rb}}$ are representative of the stages in the exchange of position between the two species associated with RTI. The components of the amplitude are $u_1 = u_{^{85}\mathrm{Rb}}$, $v_1 = v_{^{85}\mathrm{Rb}}$, $u_2 = u_{^{87}\mathrm{Rb}}$ and $v_2 = v_{^{87}\mathrm{Rb}}$. The figures correspond to (a)-(d) $a_{85}$=25$a_0$, (e)-(h)$a_{85}$=75$a_0$, (i)-(l)$a_{85}$=100$a_0$ and (m)-(p) $a_{85}$=180$a_0$. The values of $u$ and $v$ are in units of $a_{\mathrm{osc}}^{-1}$, and $x$ and $y$ are measured in units of $a_{\mathrm{osc}}$.

than number of atoms in experimentally realized TBECs, but this does not affect the qualitative nature of the present results. To form a quasi-2D trap we set $\lambda = 12.5$ and $\omega_x = \omega_y = \omega_\perp = 2\pi \times 8.0$ Hz [32]. At zero temperature, for these set of parameters, at low values of $a_{11}$ ($a_{11}$¡$a_{22}$) the $^{85}$Rb -$^{87}$Rb TBEC is in an immiscible phase with shell structured density profiles. In the domain $a_{11} < a_{22}$, the $^{85}$Rb condensate lies at the center of the trap with $^{87}$Rb condensate lying at the edges, and the positions get interchanged when $a_{11} > a_{22}$.

In Fig. 1 we show the condensate density profiles along $x$-direction as $a_{11}$ is varied from $25a_0$ to $180a_0$. Since the condensate densities follow the azimuthal symmetry of the trapping potential in the $x-y$ plane, the corresponding density profiles along $y$ direction is identical to the density along $x$-axis. In the figure, Fig. 1(a)-(b) $a_{11} < a_{22}$, $^{87}$Rb surrounds $^{85}$Rb, and in Fig. 1(c)-(d), we observe the reverse configuration as $a_{11} > a_{22}$. These are the energetically favorable density configurations. Furthermore significant changes in density profiles in Fig. 1(a)-(b) are worth notable with the increase of $a_{11}$. As $a_{11}$ is increased, an important phenomenon occurs when $a_{11}$ is larger than $a_{22}$. Around this point Rayleigh Taylor instability (RTI) sets in as the two condensates swap their positions. This is reflected in the nature of the mode evolutions, and the presence of modes with complex eigenvalues. In the density profiles, as mentioned before, the interchange of the positions is evident when we compare the density profiles in Fig. 1(b) and Fig. 1(c).

In Fig. 2 we show the evolution of the mode energies as a function of $a_{11}$. The excitation spectrum has two Kohn modes, one each for the two species. The energy of one of the Kohn modes remains constant at $\omega = \omega_\perp$ in the entire range of $a_{11}$ considered, validating Kohn's theorem, and provides an important consistency check for our computations. At the outset, when $a_{11} = 5a_0$, that is, when the TBECs are strongly phase-segregated, the energy of the other or second Kohn mode is $\omega = 0.398\omega_\perp$. With the increase in $a_{11}$, the spatial extent of $^{85}$Rb condensate gets larger, thereby leading to a finite overlap between the two species. This influences the energy of the second Kohn mode which starts becoming soft, and eventually becomes a zero energy mode when $a_{11} \approx 40a_0$ as shown in Fig. 2. The softened Kohn mode continues to be a zero energy mode till $a_{11} \approx 145a_0$ after which it regains energy and hardens. The appearance of this additional zero energy mode in the region $40a_0 \leqslant a_{11} \leqslant 145a_0$ is an indication of the onset of energetic instability within the mixture, since in the region around $a_{11} = 100a_0$, the species are expected to have RTI to minimize the total energy of the system. The onset of the RTI is also evident from the nature of the Kohn mode energy. Albeit in Fig. 2 we have plotted the real part of the Kohn mode energy, in the domain $40a_0 \leqslant a_{11} \leqslant 145a_0$ the mode energy has a small imaginary component, and this is a characteristic signature of an instability present in the system. Furthermore, our studies reveal that the quadrupole mode becomes soft with the increase in $a_{11}$, and at $a_{11} \approx 99a_0$ it becomes a zero energy mode. So, at $a_{11} \approx 99a_0$, in addition to the Nambu-Goldstone modes of the system, there are two more zero energy modes. It must be mentioned that, the quadrupole mode in the initial stages of evolution collides with the Kohn mode of the system. After the collision, its energy continues to decrease till it becomes zero energy mode, and afterwards the energy increases. The softening of the Kohn and quadrupole modes are accompanied by structural changes in the mode structures, and trends in the mode energy evolutions are a consequence of the instability in the system.

To examine the evolution of the Kohn mode in better detail

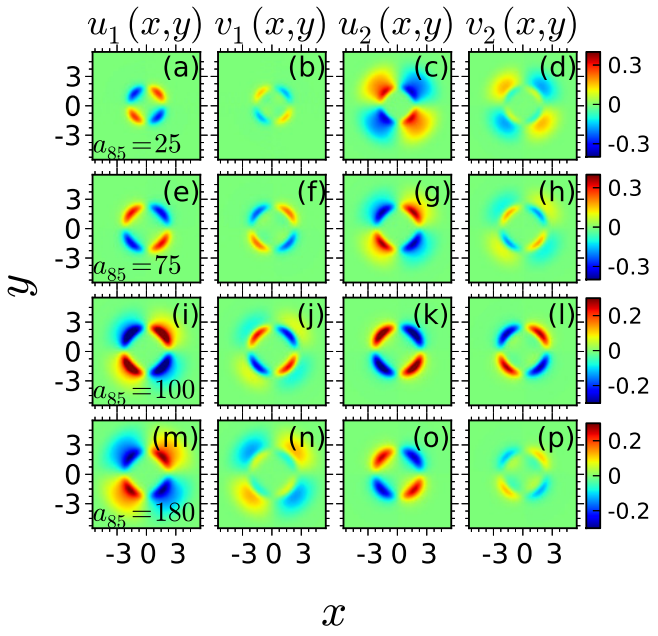


FIG. 4. (Color online) The quadrupole mode amplitude at selected values of $a_{s5_{\rm Rb}}$, and the other scattering lengths are kept fixed. The chosen values of $a_{s5_{\rm Rb}}$ are representative of the stages in the exchange of position between the two species associated with RTI. The components of the amplitude are $u_1 = u_{s5_{\rm Rb}}$, $v_1 = v_{s5_{\rm Rb}}$, $u_2 = u_{s7_{\rm Rb}}$ and $v_2 = v_{s7_{\rm Rb}}$. As $a_{s5\,Rb}$ is increased the effective wavelength of $u_1$ and $v_1$ increases whereas the reverse happens for $u_2$ and $v_2$. The figures correspond to (a)-(d) $a_{85}$=25$a_0$, (e)-(h)$a_{85}$=75$a_0$, (i)-(l)$a_{85}$=100$a_0$ and (m)-(p) $a_{85}$=180$a_0$. The values of $u$ and $v$ are in units of $a_{\rm osc}^{-1}$, and $x$ and $y$ are measured in units of $a_{\rm osc}$.

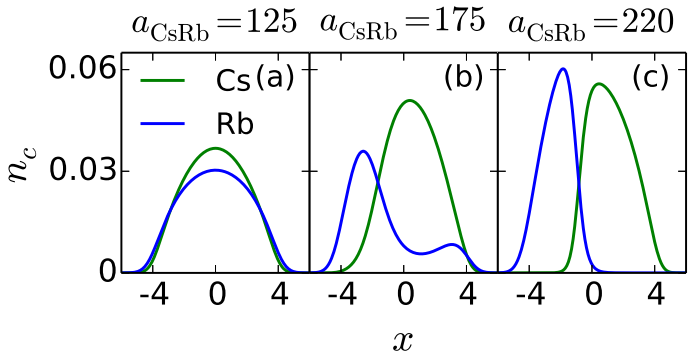


FIG. 5. (Color online) Equilibrium density profiles of Cs-Rb TBEC along $x$-axis with $y = 0$ at $T = 0$ K showing transition from miscible to immiscible (phase-separated) regimes with the change in interspecies scattering length $a_{\rm CsRb}$. (a) Shows Cs-Rb TBEC in miscible phase for $a_{\rm CsRb} = 125a_0$. (b) Corresponds to the Cs-Rb density profiles just on the verge of phase-separation at $a_{\rm CsRb} = 175a_0$. (c) Shows phase-separated density profiles of Cs-Rb TBEC for $a_{\rm CsRb} = 220a_0$. These are referred to as side-by-side density profiles. $n_c$ and $x$ are measured in units of $a_{\rm osc}^{-2}$ and $a_{\rm osc}$, respectively.

we analyse the structure of the quasiparticle amplitudes. For this we show the quasiparticle amplitude for selected values of $a_{11}$ in Fig. 3. At $a_{11} = 25a_0$, from Fig.3 (a)-(d) it is evident that the mode has a ring like geometry, and dipole in structure. With the increase of $a_{11}$ as it becomes a zero energy mode amplitude, shown in Fig.3(e)-(l), becomes broader, and this is indicative of a decrease in the wave number of the mode. At $a_{11} \approx 99a_0$, the $u_1$ and $v_1$ have a mismatch of the edges or spiral like structure, and this corresponds to the value of $a_{11}$ where the RTI is expected to occur. Finally, for $a_{11} > a_{22}$, quasiparticle amplitudes swap their position as is obvious from Fig.3(m)-(p).

An important observation associated with the quasiparticle amplitudes in Fig.3 is the relative phases of the components $u_k$ and $v_k$. For the domain $a_{11} \approx 25a_0$, shown in Fig.3(a)-(d), $u_1$ is $\pi$ out of phase with $v_1$ while $u_2$ and $v_2$ are in phase. With increase of $a_{11}$ in the domain $a_{11} \approx 75a_0$, as shown in Fig.3(e)-(h), $u_1$ and $v_1$ are in phase so are $u_2$ and $v_2$, however, $u_1$ ($v_1$) and $u_2$ ($v_2$) are out of phase. With further increase of $a_11$, at $a_{11} \approx 100$, $u_1$ is $\pi$ out of phase with $v_1$, and so are $u_2$ and $v_2$. At $a_{11} \approx 180$ when the species interchange their positions $u_1$ and $v_1$ are in phase while $u_2$ and $v_2$ are $\pi$ out of phase. Thus, not only the positions of the species, the phase difference between the quasiparticle amplitudes gets reversed. This restores the relative phase differences between the species wise quasiparticle amplitudes. The different relative phases in the domain $a_{11} \approx 75a_0$ and $a_{11} \approx 100$ are the intermediate phase patterns in the transition associated with the exchange in the position of the two species. A similar trend is observed in the case of quadrupole mode as well, and are shown in Fig.4. The variation of quasiparticle amplitudes corresponding to the quadrupole mode which has $\omega = 1.224\omega_\perp$ at $a_{11} = 5a_0$ is shown in Fig.4. We note that as $a_{11}$ is increased the effective wavelength corresponding to $u_1$ and $v_1$ increases, and the reverse happens for the $u_2$ and $v_2$. The reason is that with the increase of $a_{11}$ it is energetically favourable for the species 1 to be at the periphery and species 2 to be at the core. As discussed earlier, the changes are also manifested in the mode evolution. However, the changes in the structure, and phases of the quasiparticle amplitudes are unique characteristics associated with the onset of RTI.

### B. $^{133}$Cs-$^{87}$Rb BEC mixture

A TBEC of heteronuclear atoms, and which is of current experimental interest is Cs-Rb TBEC [33]. This experimental observation has been the stepping stone towards the realization of stable ultracold CsRb molecules in the rovibrational ground state [34, 35]. It is possible to steer this TBEC from the miscible to immiscible phase using interspecies Feshbach resonance [4]. In this system we label Cs and Rb to be species 1 and 2, respectively. With this identification $a_{11} = a_{\rm CsCs} = 280a_0$ and $a_{22} = a_{\rm RbRb} = 100a_0$, as mentioned earlier $a_0$ is the Bohr radius. For these scattering lengths, and based on Thomas-Fermi approximation, the condition for phase-separation is $a_{12} = a_{\rm CsRb} > 164a_0$, which is lower than the background $a_{\rm CsRb} \approx 650a_0$ [36]. The quasi-2D Cs-Rb TBEC system that we consider here corresponds to $N_1 = N_2 = 2000$, and the trapping parameters are the same as mentioned earlier. For this set of parameters, with

$a_{12} = 125a_0$, the ground state of the system is in miscible phase and is rotationally symmetric. The density profile is as shown in Fig. 5(a). As $a_{12}$ is increased to higher values, at the point of phase-separation the rotational symmetry is, however, broken at $a_{12} \approx 175a_0$ as shown in Fig. 5(b). The Cs-Rb condensate clouds segregate from each other at higher $a_{12}$ with minimal interfacial overlap. They lie adjacent to each other with Cs condensate cloud occupying one side of the trap, and Rb condensate cloud occupying the other side. An example of the side-by-side ground-state density profile of Cs-Rb TBEC is shown in Fig. 5(c).

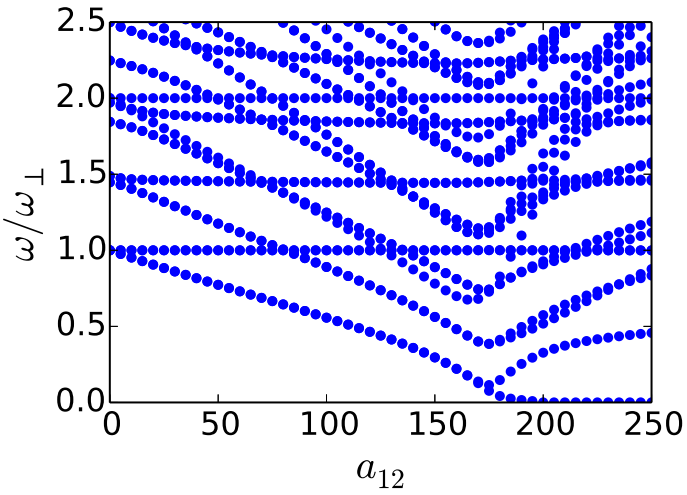


FIG. 6. (Color online) The evolution of the low-lying modes in Cs-Rb TBEC as a function of the interspecies scattering length $a_{\mathrm{CsRb}}$. Here $a_{12}$ is in units of $a_0$.

### 1. *Mode evolution for miscible to side-by-side transition*

The low-lying excitation spectra of a quasi-2D TBEC system is described by the presence of two Goldstone modes, and the degenerate slosh or dipole modes. The slosh modes of the two condensates may either be out-of-phase or in-phase. The in-phase slosh modes with center-of-mass motion are referred to as Kohn modes. To investigate the interaction induced modification of the quasiparticle spectra due to phase transition from miscible to immiscible regimes, we vary $a_{\mathrm{CsRb}}$ and compute the quasiparticle energies at zero temperature. At the outset, when $a_{\mathrm{CsRb}} = 0$, Eqns. (2) become decoupled and the excitation spectrum of the two species are independent. The slosh modes of the system then occur at $\omega = \omega_\perp$. These modes, however, start intermixing for $a_{\mathrm{CsRb}} > 0$. With increasing $a_{\mathrm{CsRb}}$, the energy of the slosh mode decreases, but the Kohn mode remains steady at $\omega = \omega_\perp$. At higher $a_{\mathrm{CsRb}}$, the energy of the doubly degenerate slosh modes decreases further till it attains a minimum value at $a^{\mathrm{c}}_{\mathrm{CsRb}} \approx 175a_0$. The rotational symmetry of the condensate is then broken at $a^{\mathrm{c}}_{\mathrm{CsRb}}$, and the degeneracy of the slosh modes is lifted, accompanied by the bifurcation of the mode energy into two branches. For $a_{\mathrm{CsRb}} > 175a_0$, the Cs-Rb density profiles start segregating from each other till they become phase-separated at $a_{\mathrm{CsRb}} \approx 220a_0$ as shown in Fig. 5(c). With the variation of $a_{\mathrm{CsRb}} = 175a_0$ to $a_{\mathrm{CsRb}} = 220a_0$, the energy of the quasiparticle excitation corresponding to the lower branch continues to go soft and becomes a Goldstone mode. The upper branch, however, hardens. This trend in mode evolution is shown in Fig. 6.

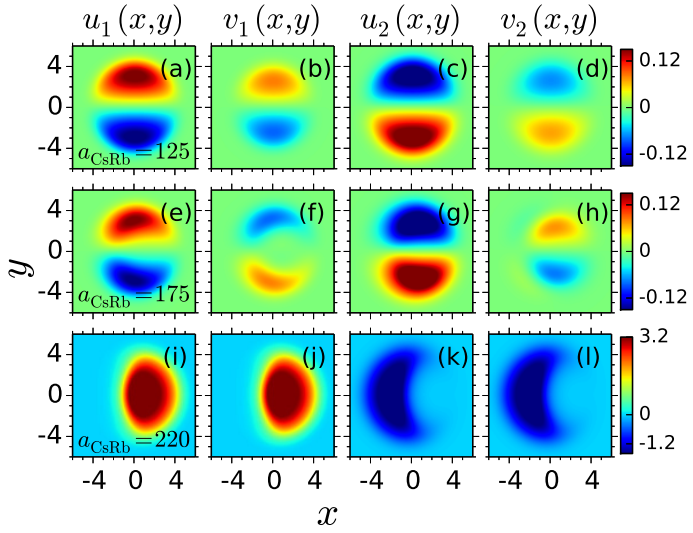


FIG. 7. (Color online) Evolution of the quasiparticle amplitudes corresponding to the slosh modes whose energy decreases as $a_{\mathrm{CsRb}}$ is varied from $0a_0$ to $250a_0$. (a-d) show the quasiparticle amplitudes corresponding to one of the degenerate Kohn modes at $a_{\mathrm{CsRb}} = 125a_0$. At $a_{\mathrm{CsRb}} = 175a_0$, that is, at the point of phase-separation, the degeneracy of the Kohn mode is lifted and a bifurcation in the mode evolution is evident. The quasiparticle amplitudes corresponding to the lower branch of the slosh mode are shown in (e-h) for $a_{\mathrm{CsRb}} = 175a_0$, and (i-l) for $a_{\mathrm{CsRb}} = 220a_0$. Here $u$s and $v$s are in units of $a_{\mathrm{osc}}^{-1}$. $x$ and $y$ are measured in units of $a_{\mathrm{osc}}$.

The transformation of the condensate density profiles leads to the modification of the structure of quasiparticle amplitudes as shown in Figs. 7, 8. These amplitudes correspond to the slosh mode. We show that the metamorphosis of the quasiparticle amplitudes corresponding to the two branches are dramatically different as the degeneracy of the slosh mode gets lifted at the point of phase-separation. When $a_{\mathrm{CsRb}} = 125a_0$, the condensates are miscible, and the slosh modes are degenerate with the same $|u_{\mathrm{Cs}}|$ and $|u_{\mathrm{Rb}}|$, but are out-of-phase with each other. However, $|u_{\mathrm{Cs(Rb)}}| > |v_{\mathrm{Cs(Rb)}}|$ as shown in Figs. 7(a)-(d), 8(a)-(d). At $a_{\mathrm{CsRb}} \approx 175a_0$, the rotational symmetry of the ground state is broken, and the condensates begin to phase-separate with the development of an interface. As mentioned earlier, the slosh mode bifurcates into two branches. The Bogoliubov quasiparticle amplitudes corresponding to the lower energy branch are shown in Fig. 7(e)-(h). The deformation of the slosh modes with the breaking of rotational symmetry is evident. Here too $|u_{\mathrm{Cs(Rb)}}| > |v_{\mathrm{Cs(Rb)}}|$, but are out-of-phase with each other. For the amplitudes corresponding to the upper branch, the dipole nature of the modes begins to cease in $u_{\mathrm{Cs}}$ and $v_{\mathrm{Cs}}$, and becomes almost single-lobed as shown in Fig. 8(e)-(f). Similar symmetry-broken structural deformation is demon-

strated in $u_{\rm Rb}$ and $v_{\rm Rb}$ as shown in Fig. 8(g)-(h). After phase-separation, that is when $a_{\rm CsRb} > 175a_0$, the non-degenerate slosh modes represent both bulk and interface excitations. One of the slosh modes belonging to the lower branch gets transformed to a Goldstone mode, and the amplitude of this mode, at $a_{\rm CsRb} \approx 220a_0$, resembling the condensate density profiles are as shown in Fig. 7(i)-(l). The upper branch, after phase-separation, corresponds to the out-of-phase quasiparticle amplitudes describing the interface excitations which are localized along the interface separating the condensates. These are shown in Fig. 8(i)-(l).

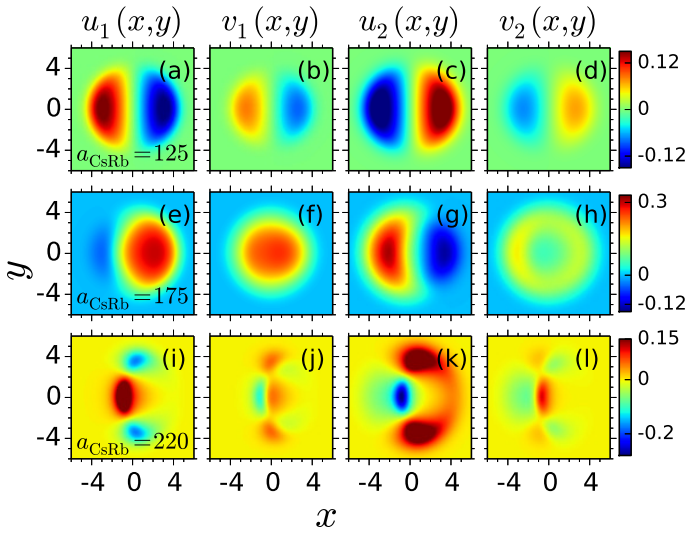


FIG. 8. (Color online) Evolution of the quasiparticle amplitudes corresponding to the slosh modes whose energy decreases as $a_{\rm CsRb}$ is varied from $0a_0$ to $250a_0$. (a-d) show the quasiparticle amplitudes corresponding to one of the degenerate Kohn modes at $a_{\rm CsRb} = 125a_0$. At $a_{\rm CsRb} = 175a_0$, that is, at the point of phase-separation, the degeneracy of the Kohn mode is lifted and a bifurcation in the mode evolution is evident. The quasiparticle amplitudes corresponding to the upper branch of the slosh mode are shown in (e-h) for $a_{\rm CsRb} = 175a_0$, and (i-l) for $a_{\rm CsRb} = 220a_0$. Here $u$s and $v$s are in units of $a_{\rm osc}^{-1}$. $x$ and $y$ are measured in units of $a_{\rm osc}$.

### 2. *Mode evolution for miscible to shell-structure transition*

For higher number of atoms and higher $\omega_z$, the density profiles of the condensates acquire a different structure during the miscible-immiscible transition with variation in $a_{\rm CsRb}$. The structure is like a shell, where the Cs atoms occupy the center of the trap, and Rb atoms occupy the edges. This configuration emerges as the energetically favourable solution for intermediate values of $a_{\rm CsRb}$. However, for large $a_{\rm CsRb}$ the shell structured profiles get transformed to side-by-side density profiles. In which Cs atoms occupy one side of the trap, and Rb atoms occupy the other side. One typical example to demonstrate this trend in the evolution of density profiles is to consider $N_{\rm Cs} = N_{\rm Rb} = 5000$. The trapping parameters are $\omega_\perp = 2\pi \times 8.0$ Hz, and $\omega_z = 2\pi \times 200$ Hz which satisfy the quasi-2D condition, that is $\mu_k \ll \hbar\omega_z$. For this set of parameters, when $a_{\rm CsRb} = 100a_0$, the ground state of Cs-Rb mixture is in miscible phase. With increasing $a_{\rm CsRb}$, the Rb condensate develops a dip at the center and becomes broader. At the point of phase-separation, that is when $a_{\rm CsRb} \approx 200a_0$, shell structured density profiles emerge as the ground state with Cs atoms at the center surrounded by Rb atoms. Here, as mentioned earlier, the condensates assume a shell structure configuration for a narrow range of $200a_0 \leqslant a_{\rm CsRb} \leqslant 205a_0$. That is to say, with a slight increase in $a_{\rm CsRb}$ the side-by-side density profiles are the energetically favourable ones. These variations in density distribution of the TBEC upon increase in $a_{\rm CsRb}$ are shown in Fig. 9.

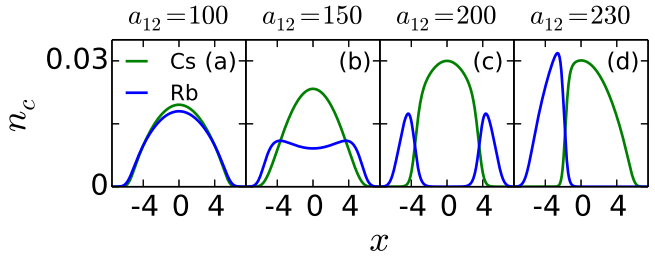


FIG. 9. (Color online)Equilibrium density profiles of Cs-Rb TBEC along $x$-axis with $y = 0$ at $T = 0$ K showing transition from miscible to sandwich to side-by-side configuration with the change in interspecies scattering length $a_{\rm CsRb}$. (a, b) Shows Cs-Rb TBEC in for $a_{\rm CsRb} = 100a_0, 150a_0$ respectively. (c) Shows the phase-separated density profiles of Cs-Rb TBEC for $a_{\rm CsRb} = 200a_0$. These are referred to as sandwich type density profiles. (d) Shows the phase-separated density profiles of Cs-Rb TBEC for $a_{\rm CsRb} = 230a_0$. These are referred to as side-by-side density profiles. $n_c$ and $x$ are measured in units of $a_{\rm osc}^{-2}$ and $a_{\rm osc}$, respectively.

With the change in $a_{\rm CsRb}$, like in the previous case, the energy of the Kohn mode remains constant throughout the evolution. The energy of the slosh mode, however, decreases. For $a_{\rm CsRb} > 200a_0$, the degeneracy of the slosh modes gets lifted giving rise to a bifurcation as shown in Fig. 10, and one of the slosh modes is transformed to a Goldstone mode of the system. The energy of the other slosh mode hardens indicating a symmetry breaking. This also reflected in the condensate density profiles, as mentioned earlier, in this domain of $a_{\rm CsRb}$ the condensate density profiles has side-by-side geometry. Another indication in the excitation spectrum is the discontinuity as shown in Fig. 10. Following this evolution, the Bogoliubov quasiparticle amplitudes corresponding to the slosh mode undergo a significant change. When the condensates are partially miscible, the slosh modes are degenerate with same $|u_{\rm Cs}|$ and $|u_{\rm Rb}|$ but are out-of-phase with each other. However, $|u_{\rm Cs(Rb)}| > |v_{\rm Cs(Rb)}|$ as shown in Figs. 11(a)-(d), (e)-(h) for two different values of $a_{\rm CsRb}$. Furthermore, at $a_{\rm CsRb} \approx 200a_0$, $|u_{\rm Cs}| < |u_{\rm Rb}|$ and are out-of-phase with each other, and the slosh mode is deformed to an excitation along the axis of the shell. These transformations of quasiparticle amplitudes are shown in Fig. 11(i)-(l). With a slight increase in $a_{\rm CsRb}$, when the rotational symmetry is broken and as discussed earlier, the slosh mode bifurcates to become a Goldstone mode, and a higher excited mode representing the excitations along the interface of the condensate. For exam-

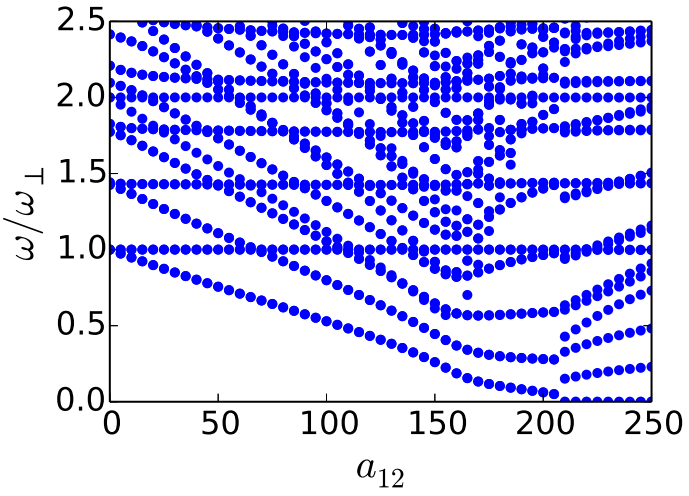


FIG. 10. (Color online)The evolution of the low-lying modes in Cs-Rb TBEC corresponding to the transition shown in Fig. 9 as a function of the interspecies scattering length $a_{\mathrm{CsRb}}$. Here $a_{12}$ is in units of $a_0$.

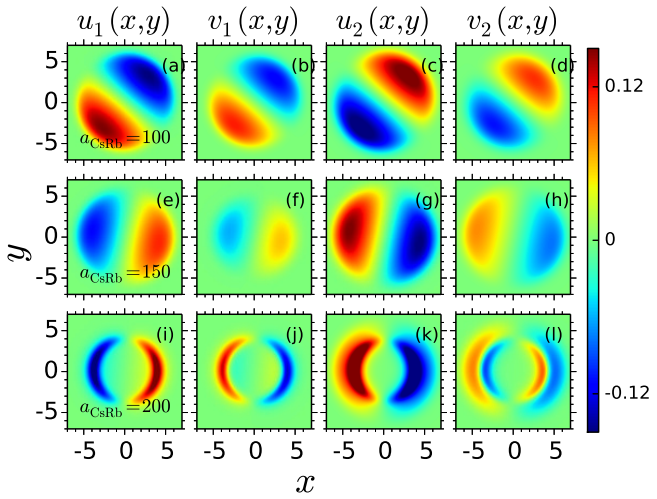


FIG. 11. (Color online) Evolution of the quasiparticle amplitudes corresponding to the slosh modes whose energy decreases as $a_{\mathrm{CsRb}}$ is varied from $0a_0$ to $250a_0$. (a-d) show the quasiparticle amplitudes corresponding to one of the degenerate slosh modes at $a_{\mathrm{CsRb}} = 100a_0$. (e)-(h) show the quasiparticle amplitudes at $a_{\mathrm{CsRb}} = 150a_0$ when the condensates are partially miscible. (i)-(l) Shown here are the quasiparticle amplitudes corresponding to $a_{\mathrm{CsRb}} = 200a_0$. Here $u$s and $v$s are in units of $a_{\mathrm{osc}}^{-1}$. $x$ and $y$ are measured in units of $a_{\mathrm{osc}}$.

ple, when $a_{\mathrm{CsRb}} \approx 230a_0$, one of the slosh modes which have become the new Goldstone mode resembles the ground state density profiles as shown in Fig. 12(a)-(d). The other one corresponding to the out-of-phase interface excitations is shown in Fig. 12(e)-(h).

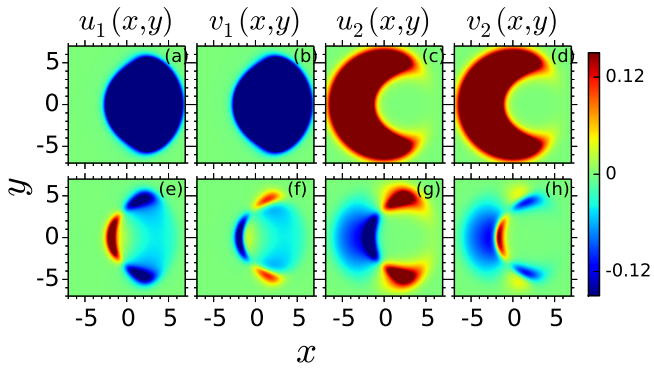


FIG. 12. (Color online) Quasiparticle amplitudes corresponding to (a)-(d) the Goldstone mode, and (e)-(h) the interfacial excitations at $a_{\mathrm{CsRb}} = 230a_0$. Here $u$s and $v$s are in units of $a_{\mathrm{osc}}^{-1}$. $x$ and $y$ are measured in units of $a_{\mathrm{osc}}$.

## IV. CONCLUSIONS

The present studies reveal unique features in the nature of quasiparticle excitation spectrum of TBECs. In the immiscible domain, the position swapping of the constituent species in a $^{85}$Rb-$^{87}$Rb mixture, which is driven by tuning intraspecies scattering length of $^{85}$Rb, is accompanied by the softening of slosh and quadrupole modes. These modes on getting softened transform to zero energy modes at the point of equal intraspecies scattering lengths. These modes harden when the intraspecies scattering lengths $^{85}$Rb increased to values higher than that of $^{87}$Rb.

For the Cs-Rb condensate mixture, where the atomic masses of the constituents are widely different, we find a different trend in the mode evolution spectrum. On steering the system from miscible to immiscible domain by tuning the interspecies scattering length, the slosh mode softens. The emergence of side-by-side density profiles as a result of phase-separation is indicated by the breaking of the rotational symmetry, and the bifurcation of degenerate slosh modes. The bifurcation gives rise to two branches, of which, one becomes the Goldstone mode of the system. Furthermore, the side-by-side density profile may also emanate from a shell structured density profile indicated by a marked discontinuity in the excitation spectrum. The variation in the quasiparticle excitations will lead to differences in the non-condensate density distributions, and dynamical structure factor which shall be investigated in our future works.

## ACKNOWLEDGMENTS

We thank K. Suthar, S. Bandyopadhyay and R. Bai for useful discussions. The results presented in the paper are based on the computations using the 3TFLOP HPC Cluster at Physical Research Laboratory, Ahmedabad, India.

[1] H. Pu and N. P. Bigelow, Phys. Rev. Lett. **80**, 1134 (1998).
[2] E. Timmermans, Phys. Rev. Lett. **81**, 5718 (1998).
[3] S. B. Papp and C. E. Wieman, Phys. Rev. Lett. **97**, 180404 (2006).
[4] K. Pilch, A. D. Lange, A. Prantner, G. Kerner, F. Ferlaino, H.-C. Nägerl, and R. Grimm, Phys. Rev. A **79**, 042718 (2009).
[5] S. B. Papp, J. M. Pino, and C. E. Wieman, Phys. Rev. Lett. **101**, 040402 (2008).
[6] S. Tojo, Y. Taguchi, Y. Masuyama, T. Hayashi, H. Saito, and T. Hirano, Phys. Rev. A **82**, 033609 (2010).
[7] D. J. McCarron, H. W. Cho, D. L. Jenkin, M. P. Köppinger, and S. L. Cornish, Phys. Rev. A **84**, 011603(R) (2011).
[8] A. Griffin, Phys. Rev. B **53**, 9341 (1996).
[9] C. Gies, B. P. van Zyl, S. A. Morgan, and D. A. W. Hutchinson, Phys. Rev. A **69**, 023616 (2004).
[10] C. Gies, M. D. Lee, and D. A. W. Hutchinson, J. Phys. B **38**, 1797 (2005).
[11] D. A. W. Hutchinson, E. Zaremba, and A. Griffin, Phys. Rev. Lett. **78**, 1842 (1997).
[12] S. Gautam and D. Angom, Phys. Rev. A **81**, 053616 (2010).
[13] T. Kadokura, T. Aioi, K. Sasaki, T. Kishimoto, and H. Saito, Phys. Rev. A **85**, 013602 (2012).
[14] M. O. C. Pires and E. J. V. de Passos, Phys. Rev. A **77**, 033606 (2008).
[15] A. Roy, S. Gautam, and D. Angom, Phys. Rev. A **89**, 013617 (2014).
[16] A. Roy and D. Angom, Phys. Rev. A **90**, 023612 (2014).
[17] A. Roy, S. Gautam, and D. Angom, Eur. Phys. J. Sp. Top. **224**, 571 (2015).
[18] A. Roy and D. Angom, New J. Phys. **18**, 083007 (2016).
[19] B. Hu, G. Huang, and Y.-l. Ma, Phys. Rev. A **69**, 063608 (2004).
[20] Y. Japha and Y. B. Band, Phys. Rev. A **84**, 033630 (2011).
[21] C. Ticknor, Phys. Rev. A **88**, 013623 (2013).
[22] C. Ticknor, Phys. Rev. A **85**, 033629 (2012).
[23] S. L. Cornish, N. R. Claussen, J. L. Roberts, E. A. Cornell, and C. E. Wieman, Phys. Rev. Lett. **85**, 1795 (2000).
[24] J. L. Roberts, N. R. Claussen, J. P. Burke, C. H. Greene, E. A. Cornell, and C. E. Wieman, Phys. Rev. Lett. **81**, 5109 (1998).
[25] T.-L. Ho and V. B. Shenoy, Phys. Rev. Lett. **77**, 3276 (1996).
[26] R. Lehoucq, D. Sorensen, and C. Yang, *ARPACK Users' Guide* (Society for Industrial and Applied Mathematics (Philadelphia), 1998).
[27] T. Simula, S. Virtanen, and M. Salomaa, Comput. Phys. Commun. **142**, 396 (2001).
[28] W. Kohn, Phys. Rev. **123**, 1242 (1961).
[29] L. Brey, N. F. Johnson, and B. I. Halperin, Phys. Rev. B **40**, 10647 (1989).
[30] J. F. Dobson, Phys. Rev. Lett. **73**, 2244 (1994).
[31] A. L. Fetter and D. Rokhsar, Phys. Rev. A **57**, 1191 (1998).
[32] T. W. Neely, E. C. Samson, A. S. Bradley, M. J. Davis, and B. P. Anderson, Phys. Rev. Lett. **104**, 160401 (2010).
[33] R. W. Pattinson, T. P. Billam, S. A. Gardiner, D. J. McCarron, H. W. Cho, S. L. Cornish, N. G. Parker, and N. P. Proukakis, Phys. Rev. A **87**, 013625 (2013).
[34] P. D. Gregory, J. Aldegunde, J. M. Hutson, and S. L. Cornish, Phys. Rev. A **94**, 041403(R) (2016).
[35] P. K. Molony, P. D. Gregory, Z. Ji, B. Lu, M. P. Köppinger, C. R. Le Sueur, C. L. Blackley, J. M. Hutson, and S. L. Cornish, Phys. Rev. Lett. **113**, 255301 (2014).
[36] A. Lercher, T. Takekoshi, M. Debatin, B. Schuster, R. Rameshan, F. Ferlaino, R. Grimm, and H.-C. Nägerl, Eur. Phys. J. D **65**, 3 (2011).